

POLITECNICO DI TORINO

Department of Electronics and Telecommunications

Master's Degree program in
ICT for Smart Societies

Master Thesis

**Magnetic Sensor Array System:
an Innovative Approach to Train
Localization**



Supervisor
Prof. Fabio DAVIS

Candidate
Stefano Callaris

April 2019

Abstract

In a railway environment, train localization is necessary to have a safe and efficient traffic within the railway network of tracks. This work presents a study regarding a magnetic sensor system, which is used for train localization. At present, train position is usually determined by computing the travelled distance from the last beacon, using a wheel-turn counter. So far, this localization system has been the best solution for environments where satellite localization is not available, as for example in tunnels.

Train localization using magnetic sensors achieves performances similar to satellite localization. Besides, magnetic localization does not rely on additional infrastructure on the track-side and it is always available. During this work, a system based on multiple low-cost magnetic sensors has been designed, built and tested. The result is the *magnetic sensor array system*: an on-board train localization system with accuracy comparable to the satellite localization based systems.

This work has a threefold objective. First, to test if accurate train localization is achievable with low-cost magnetic sensors. Second, to determine if the combined use of multiple magnetic sensors can improve the localization accuracy performances. Third, to determine if it is possible to recognize and exclude the magnetic field distortion caused by a neighboring train.

A first experiment was conducted to answer the first two questions. According to the results, a single low cost sensor is not enough to achieve accurate localization, but the combined used of multiple low-cost sensor provides reliable information to train localization. When matching the last 30 meters of collected magnetic data, the single sensor provided the right train position on 80% of the time, while the multiple sensor system provided the correct position on 99% of the time on the single measurement.

A second experiment investigated the decay of the magnetic field disturbance caused by a neighboring train on a standard train-to-train distance across two parallel tracks. According to the obtained results, the magnetic influence on the external side is reduced down to 20% with respect to the internal side, making it possible to detect and exclude the neighboring train disturbance.

ACKNOWLEDGMENT

I would like to thank the German Aerospace Center for welcoming me during the last part of my academic education. The work of thesis would not have been as valuable to me without their support. In particular, my gratitude goes to my tutor Oliver Heirich, who has been an excellent mentor and has guided me through the long and complex path of this thesis.

I would also like to thank my academic supervisor Fabio Dosis. His constant support and gentle suggestions have been to me of extremely valuable during the months of the thesis. He has always been present for help and advice, and of that I am profoundly grateful.

Contents

1	Introduction	5
1.1	Thesis objective	5
1.2	State-of-the-Art and Previous Works	6
1.3	Thesis Outline	7
2	System Design	9
2.1	General Description and Requirements	9
2.2	Hardware Design	11
2.2.1	Sensor Choice	11
2.2.2	Sensor Element	13
2.2.3	Array Controller	14
2.2.4	Array Interface	15
2.3	Software Design	17
2.3.1	Sensor Element	17
2.3.2	Array Controller	20
2.3.3	Data Processing	22
3	Calibration	25
3.1	Calibration Method	25
3.1.1	Magnetic Field Measurement Model	25
3.1.2	Evaluation of Calibration Parameters	26
3.2	Calibration Setup	27
3.3	Results and Discussion	28
4	Magnetic Localization	31
4.1	Experimental setup	31
4.2	Methods	33
4.2.1	Data Conversion: from Time to Space Domain	33
4.2.2	Position Estimation Methods	35
4.2.3	Evaluation of Localization Accuracy	37
4.3	Results and Discussion	37
4.3.1	Methods' Performance and Comparison	37
4.3.2	Performance Comparison of PNI and KMX sensors	41

5	Neighboring Train Disturbance Analysis	43
5.1	Experimental Setup	43
5.2	Methods	44
5.3	Results and Discussion	47
6	Conclusions	51

Chapter 1

Introduction

Railway is one of the main and most developed land transport systems [1]. It is used for goods and people displacement, and it is scaled both on local and international level. Key features of a railway network are safety and efficiency. Safety is about avoiding train collision and accidents. For example, collisions are prevented by a network protocol which guarantees exclusive access to every track section. In this way, it is certain that two trains cannot run on the same track section at the same time. Efficiency is about reaching the maximum possible system exploitation, with an adequate management and use of the track network.

Train localization is critical in railway control system. Knowing each train position helps in avoiding collisions and making the whole system more efficient. Eventually, an accurate knowledge of the system state is necessary to increase the network utilization without compromising its safety.

Train localization can be achieved with two different approaches. The first one is the *infrastructure-based* approach: the train localization is obtained exploiting dedicated items of the infrastructure. The second one is the *infrastructure-less* approach: the localization system is an on-board system and it does not require dedicated items of the infrastructure.

The position of a train is tied to the track network. In order to achieve train localization, two pieces of information are required: the track ID and the 1-D position on that track. The train position along a track is referred as the *along-track train localization* parameter. The track ID instead refers to the *cross-track train localization*. In case of parallel tracks, cross-track localization states which track is occupied by the train.

1.1 Thesis objective

This thesis focuses on the use of a magnetic sensor system for train localization. The considered system adopts the infrastructure-less approach. Considering the available literature about magnetic sensor systems [2, 3, 4],

this work has three main objectives.

The first aim is to build a system which is low cost and easily scalable. In previous works the adopted magnetic sensor system was too much expensive to allow this technology to spread. This work aims to investigate if magnetic localization can be achieved through low cost sensor, without compromising accuracy. The second aim is to understand if multiple magnetic sensor can provide a better position estimation accuracy than a single sensor system. The third aim is to investigate how the magnetic field differs along the cross track direction. In particular, the focus is about understanding if the magnetic influence of a neighboring train can be recognized and excluded from the magnetic data used for train position estimation.

1.2 State-of-the-Art and Previous Works

The state of the art for most railways network worldwide is an infrastructure based approach: The train is spotted at its passage through stations and critical points, tracking the train position in a discrete way. Each train is equipped with a wheel-turn counter, that provides the travelled distance and the train speed. The on-board gathered information, however, is often used only by the train driver at a local level.

Besides, counting the turns of the wheel is not an accurate way to estimate position and velocity: the wheel diameter changes according to temperature and its wear condition; The wheel itself might slide on the track when breaking, introducing measurement errors.

Train localization has been investigated through multiple approaches and multiple sensor systems. The most promising results come from the Global Navigation Satellite System (GNSS) localization [5, 6], the eddy current sensor systems [7, 8], and the magnetic sensor systems [2, 3, 4]. GNSS has good accuracy performances regarding the along-track localization, but is not accurate enough regarding the cross-track localization. What's more, it's availability is not guaranteed and indeed it is compromised in specific environments (e.g. tunnels, forests, urban canyons).

Eddy current sensor systems measure the current induced by the moving train. The current is influenced by all ferromagnetic materials close to the track and by the track itself. This kind of system is still in the developing phase.

Magnetic sensor systems measure passively the magnetic field surrounding the train. The local magnetic field is mostly driven by the Earth's magnetic field, but all ferromagnetic materials contribute to its final value. If the environment does not change, a train passing twice in the same place will record the same variations in the magnetic field: the variation pattern can be used to identify the train position. In addition to this, [2] showed that

changing the sensor position the recorded *magnetic signature* changed consequently. The position accuracy obtained with the magnetic sensor system is encouraging, especially for the cross-track localization.

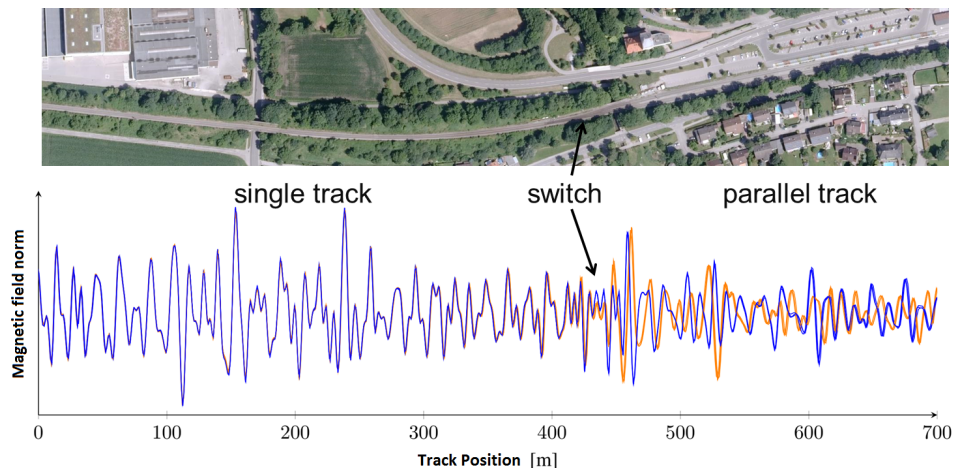


Figure 1.1: The magnetic signature is the magnetic field along a track as a function of the position [4]. Here, two different trains record the same magnetic signature when they are on the same track, but record different magnetic signature for different track path.

The magnetic field along a railway track is influenced by all the ferromagnetic materials that compose the infrastructure and in the surrounding environments. The magnetic field as a function of the position along a track is here referred as *magnetic signature*. The magnetic signature is specific and unique for each railway track. Figure 1.1 shows multiple runs of a train going along path A (with corresponding orange magnetic signature) and path B (with blue magnetic signature).

From left to right, both paths are equal until the switch point, and different from that point on. The magnetic signatures, accordingly, are similar until the switch point and different from that point on. It is worth noticing that for both path A and B multiple runs are plotted: The magnetic signature repeats itself so accurately that it is difficult to distinguish a run from another in a qualitatively way.

1.3 Thesis Outline

This thesis is structured in six chapters. Chapter 2 is about the system design, where design and implementation choices and steps are discussed. Chapter 3 is dedicated to the system calibration: it comprehends both the required theoretical background and the practical implementation. Chapter 4 is about the experiment that investigates magnetic train localization in the along-track direction. It addresses the first two objectives of this work. Chapter 5 is about the experiment that analyzes the magnetic disturbance

magnitude along the cross-track direction. It addresses the third objective of this work. Chapter 6 draws the conclusions for the overall work and suggests possible developments in this research stream.

Chapter 2

System Design

2.1 General Description and Requirements

The Magnetic Sensor Array System (MSAS) is an on-board localization system designed for railway environment. The MSAS measures both magnetic field intensity and acceleration. The system is composed of three sub-systems: sensor element, array controller, array connection. Figure 2.1 shows the MSAS idea: 11 sensor elements are connected to the array controller through the array connection unit.

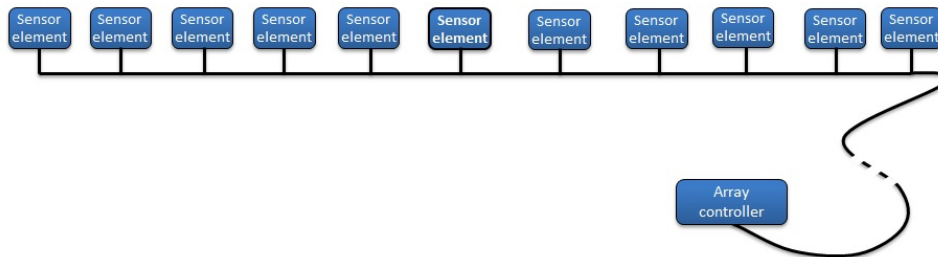


Figure 2.1: Abstract MSAS scheme.

A few requirements have been determined before starting with the design process of the MSAS:

- operating sampling frequency: in order to have an accurate representation of the magnetic field variations in the railway context, the sampling frequency of the system is 200 Hz
- magnetic sensors used in the MSAS should be in the low-cost range, to allow the system to match the market demand
- magnetic sensor must have sensitivity on the 100 nT range or below, to be able to measure accurately the target signals.

- the hardware setup must be robust enough to undergo the physical stress caused by railway environment
- communication protocols resilient to electromagnetic interference

Each sensor element is a complex unit, able to perform measurements and answer back to the array controller request. The sensor elements are all equal except the central one, which is additionally equipped with an Inertial Measurement Unit (IMU). The sensor element components are analyzed in detail in Section 2.2.2, while this Section presents a generic overview of the sensor element components and allocation. All sensor element units are equipped with 2 magnetic sensor, KMX and PNI. Refer to Section 2.2.1 for sensor details. Figure 2.2 shows a standard sensor element: The PNI breakout board is on the top of the unit, on the left side. The KMX sensor is underneath, close to the left border of the unit. The microprocessor is by the board center. The power unit and the external connections are on the side opposite to the magnetic sensor's, in order to minimize electromagnetic interference due to flowing currents.

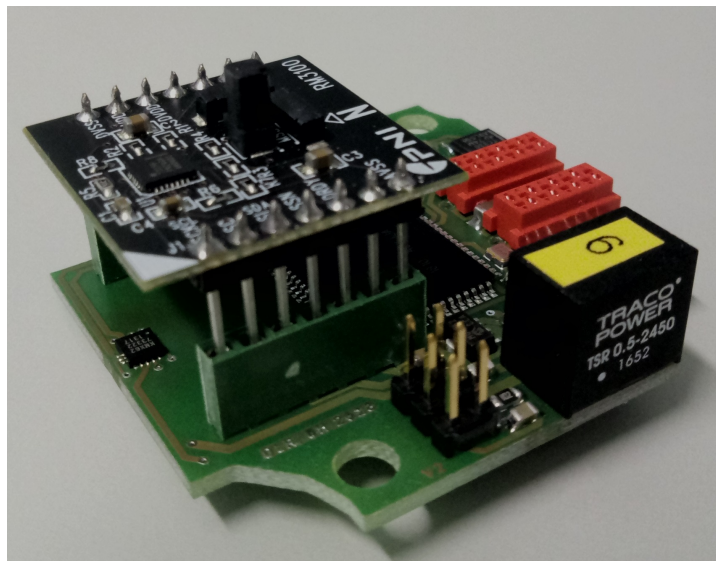


Figure 2.2: Electronic circuit board of the sensor element: top left is the PNI sensor, underneath it the KMX sensor.

The array controller powers up the whole array. The array controller is able to: trigger a measurement event for all sensor elements; receive all messages from the sensor elements and forward them to a computer; change initialization settings in the sensor element regarding sampling requirements and routines.

All sensor elements are mounted on an a-magnetic aluminum pole, and are placed inside aluminum boxes. The sensor elements are connected to the array controller by a unique cable. This cable contains two wires for power supply, two wires for the Controller area network (CAN) bus communication [9], two wires for the trigger signal, and two wires for the reset signal. The cable runs off-sight inside the MSAS and exits with no interruption from the array side, while it has a resilient connector on the array controller side. The array controller can therefore be placed at several meters from the MSAS. The complete sensor array is shown in Figure 2.3. The central sensor element, with the German Aerospace Center (DLR) logo, is the one equipped with the additional IMU.



Figure 2.3: MSAS in its operational setup: 11 boxed sensor elements are fixed on the aluminum pole.

The array connection conveys power and three communications signals between the sensor elements and the array controller. All communication signals are differential: The first is the CAN bus transmission, held according to the CAN protocol. The second is the SYNC signal, generated from the array controller, triggers the sensor elements to send a magnetic measurement on the CAN bus, according to the sensor element settings. The third is the RST signal, that resets to zero the magnetic measurement message counter inside the sensor elements.

2.2 Hardware Design

2.2.1 Sensor Choice

The first step in designing the sensor element has been to choose the magnetic sensors. The performed market review comprise 14 magnetic sensors, with different characteristics.

Figure 2.4 reports the considered sensors plotted as linear price over logarithmic magnetic resolution. As a reference, a reasonable value for the

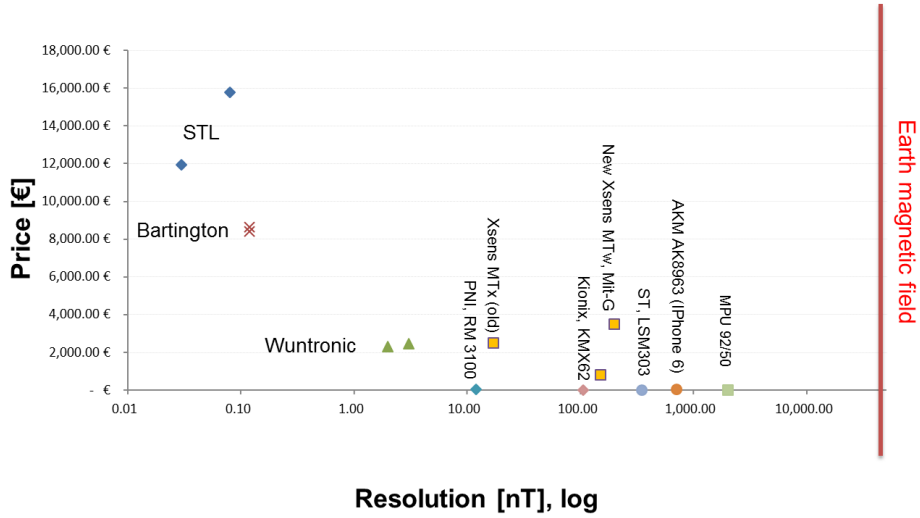


Figure 2.4: Magnetic sensor market review.

Earth’s magnetic field intensity (48 μ T) is plotted. Five sensor have prices below 50 euro each: these sensor are considered in the “low-cost” range. Six sensors have resolution below 3 nT and these sensors are defined as “reference sensors”.

All the reported sensors except the Bartington’s have been tested during the work for this thesis. The preliminary analysis have been useful to evaluate parameters not explicitly reported in all sensor datasheets, such as measurement noise over sampling frequency. Few sensors have been excluded because of their measuring range, some because they could not reach the required operating frequency. Finally, two low cost sensors and one reference sensor have been selected for this work. The choice has been driven by: price, resolution, sensibility, sampling frequency, and average measuring noise. As the system target values can be seen as differential value, the absolute accuracy is not a top-priority requirement.

The chosen reference sensor is the Wuntronic WFG-D-130 [10]. It is a digital flux-gate magnetic sensor. The reference sensor purpose is to calibrate the low-cost sensors of the MSAS. The reference sensor does not take active part in the measurement phase. The main characteristics for the reference sensor are shown in table 2.1.

The first of the chosen low-cost sensors is the PNI-RM3100 [11], referred in the following as PNI. This sensor exploits the micro-fluxgate technology for magnetic field measurements. The PNI sensor setup contains micro-coils and

an ASIC, and it is homed on a small break out board. The micro-fluxgate measures are quantized with a 24-bit ADC and gathered by a microprocessor that communicates according to the Inter-Integrated Circuit (I^2C) standard. The main parameters for the PNI sensor are shown in table 2.1.

The second chosen low-cost sensor is the KMX KMX62-1031 [12], referred in the following as KMX. This sensor is a typical smart-phone sensor: integrated chip of small dimensions (only $3\text{ mm} \times 3\text{ mm}$). Its characteristics are better than the other analyzed low-cost sensors, but definitely worse than the PNI sensor characteristics. The specifications are shown in detail in table 2.1.

Parameter	WFG	PNI	KMX
Sensitivity	3 nT	26 nT	37 nT
Noise level	$\pm 3\text{ nT}$	$\pm 20\text{ nT}$	$\pm 500\text{ nT}$
Range	$\pm 100\text{ }\mu\text{T}$	$\pm 800\text{ }\mu\text{T}$	$\pm 1200\text{ }\mu\text{T}$
Max frequency	250 Hz	340 Hz	800 Hz
Single-axis ADC output	24 bit	24 bit	16 bit

Table 2.1: Comparison of sensor specifications at operative conditions.

2.2.2 Sensor Element

The sensor element is one of the main sub-units of the MSAS. Its purpose is to measure the variations in the local magnetic field in order to perform magnetic localization. Its components are:

- magnetic sensors (PNI and KMX)
- IMU, optional (XSens MTi-1)
- microprocessor (ATMEL AT90CAN128)
- power converter, CAN transceiver, connectors and other secondary units.

The chosen micro-controller is the ATMEL AT90CAN128 [13]. It is designed to have an efficient CAN communication interface, which allows the CPU to focus on the sensor measurement reception and management. The communication between microprocessor and magnetic sensors exploits the I^2C interface, that is explicitly designed for short range communication between integrated units. The data transmission from the sensor element to the array controller exploits the CAN bus, which is designed for noisy electromagnetic environments. Some specific signals towards the sensor element have a dedicated line. Those signals are transmitted as differential

signals on two wires, to ensure resilience and also because of the multiple electric grounds in the system. The central sensor element of the MSAS is additionally equipped with the XSens MTi-1 sensor [14]. The only data gathered from the XSens unit is the acceleration measure, which can be used to determine the relative distance between the MSAS measurements.

In order to reduce the electromagnetic interference over the magnetic field measurements, the Printed Circuit Board (PCB) has been designed to have the magnetic sensors as far as possible from the power and transmission sections. Furthermore, to ensure the unit protection without affecting the magnetic field measurements, the sensor element is cased in an aluminum box, which is non ferromagnetic. The sensor element is fixed to the array structure with a single steal screw, placed as far as possible from the magnetic sensors.

2.2.3 Array Controller

The array controller has been developed in two different versions: one is based on a RaspberryPi 3, the other is based on an Arduino DUE. The RaspberryPi 3 version development was interrupted at the last stages, because the RaspberryPi unit is not suited for real-time application. In this case, It was not possible to perform error-free data transmission because of the high latency in the RasperryPi response. As an additional intermediate piece of hardware would have been needed, the RaspebbyPi-based array controller development was interrupted. The Arduino DUE version instead is perfectly able to manage the ongoing system communications. On the other hand, storing data on the Arduino DUE is not possible, thus the received magnetic data are forwarded to an external unit, i.e. the computer used for data analysis. The Arduino DUE array controller is composed by:

- standard Arduino DUE Board
- explicitly designed PCB for interfacing purposes
- explicitly designed CAN2SPI unit, for magnetic data reception
- commercial GNSS device

The main version of the array controller is based on an Arduino DUE board. On top of it, a dedicated PCB has been designed to: perform power conversion and distribution; convert output signals (CAN, SYNC, RST) from single-ended to differential; facilitate external devices connection through the CLICK interface [15] (i.e. a standardized hardware pin-mapping).

Power conversion is from 12V to both 5V and 3.3V in order to provide

power the Arduino DUE board and the connected devices. A 12 V power is supplied to the MSAS, and it is locally converted to 3.3 V by each sensor element.

There are three CLICK board connectors: one of them is dedicated to the CAN2SPI unit, while the second one connects a commercial GNSS receiver board, which is used both for localization and synchronization; the third one is reserved for future use.

The CAN2SPI unit has been designed during the work for this thesis. It has the same micro-controller and a CAN transceiver as the sensor element units. Its purpose is to receive multiple CAN messages, temporarily buffer them and forward them to the Arduino DUE board through the Serial Peripheral Interface (SPI) bus. The message forwarding can alternatively be set on the serial bus.

The GNSS commercial device is the “u-blox EVK-M8” [16]. This device is set to transmit GNSS PVT data to the Arduino board over the serial interface to the Arduino DUE. It also generates the RST and the SYNC signals. The RST signal is set at a 1 Hz frequency, while the SYNC signal is set at a 200 Hz frequency. RST and SYNC signals are generated as single-ended signals at this stage, and converted to differential signals by the array controller.

To sum up, the MSAS uses multiple communication protocols: I^2C between magnetic sensors and microprocessor, CAN between sensor element and array controller. Inside the array controller, the Arduino DUE communicates with the CAN2SPI unit over SPI protocol, and serial communication takes place with the GNSS unit. Finally, the data are forwarded to an external device (computer) over an USB connection.

The array controller is the link between the array measuring part and the external world, where the data analysis takes place. In picture 2.5 it is possible to see the complete MSAS. The picture was taken during the second experiment (Chapter 5). The sensor elements are on the aluminum pole, together with the reference sensor; the array connection links the sensor elements to the array controller, the white box at the bottom of the picture; The array controller is connected to a laptop, to allow data storage and analysis.

2.2.4 Array Interface

The array connection cable has to deliver for different signals: Power, SYNC, RST, CAN. As all those signals are differential, eight independent



Figure 2.5: Complete MSAS: The sensor array is connected through a single cable to the array controller, which is connected to the GPS antenna and to a 12 V battery that powers the whole system. The array controller is USB connected to a laptop for data storage and analysis.

lines are required. The used cable is a shielded against electromagnetic interference and it is composed by four wire twisted pairs. This type of cable is usually used for Ethernet connection. The inner cable connections have been re-mapped to match the MSAS needs.

The power flow in the system happens mainly at 12 V. The array controller is powered at 12 V and delivers the same voltage to all sensor elements. The required lower voltages of 3.3 V and 5 V are obtained locally on decoupled reference grounds. Hence, differential signals are required to broadcast the messages.

The magnetic message transmission is performed over the CAN bus [9]. The used symbol transmission rate is 1 MHz. The CAN standard transmission is composed by the user address of 11 bits and the message payload of 8 bytes. In the MSAS, every CAN message payload has the first 2 bytes dedicated to a message counter. This leaves only 6 data bytes in each message. A PNI measurement contains three 24 bit values, hence it will require 2 CAN messages. A KMX sensor measurement contains three 16 bit values, so one CAN message is used for every measurement. In addition to this, the IMU requires 2 additional CAN messages. A total number of 35 CAN messages are required to transmit the collected data at each sampling event. This results in a bus load close to 90%. The CAN implements a priority protocol in order to avoid collisions. The user priority is stated by its own CAN address.

A second kind of CAN messages is used within the MSAS is the configuration message. Configuration messages are from the array controller to the sensor element and are used to change the operational settings of the sen-

sensor elements. The payload, which is 1 byte long, contains the configuration command. Configuration messages can also be used to test one sensor element connection and operational status, blinking the sensor element LED. The CAN messages definition is shown in Figure 2.6 (Messages with Msg_ID 7 and 8 are not implemented in the current system).

Origin	Message	Msg ID	Identifier 11bit	Bytes	Byte 1	Byte 2	Byte 3	Byte 4	Byte 5	Byte 6	Byte 7	Byte 8
Sensor element	KMX62 mag meas, counter	1	0 00001 XXXXX	8	Cnt H	Cnt L	Mag X L	Mag X H	Mag Y L	Mag Y H	Mag Z L	Mag Z H
Sensor element	KMX62 acc meas, counter	2	0 00010 XXXXX	8	Cnt H	Cnt L	Acc X H	Acc X L	Acc Y H	Acc Y L	Acc Z H	Acc Z L
Sensor element	PNI meas, counter 1	3	0 00011 XXXXX	8	Cnt H	Cnt L	Mag X H	Mag X M	Mag X L	Mag Y H	Mag Y M	Mag Y L
Sensor element	PNI meas, counter 2	4	0 00100 XXXXX	8	Cnt H	Cnt L	Mag Z H	Mag Z M	Mag Z L	0	0	0
Sensor element	Xsens acc,gyr,counter 1	5	0 00101 XXXXX	8	Cnt H	Cnt L	Acc X H	Acc X MH	Acc X ML	Acc X L	Acc Y H	Acc Y MH
Sensor element	Xsens acc,gyr,counter 2	6	0 00110 XXXXX	8	Cnt H	Cnt L	Acc Y ML	Acc Y L	Acc Z H	Acc Z MH	Acc Z ML	Acc Z L
Sensor element	Xsens acc,gyr,counter 3	7	0 00111 XXXXX	8	Cnt H	Cnt L	Gyr X H	Gyr X MH	Gyr X ML	Gyr X L	Gyr Y H	Gyr Y MH
Sensor element	Xsens acc,gyr,counter 4	8	0 01000 XXXXX	8	Cnt H	Cnt L	Gyr Y ML	Gyr Y L	Gyr Z H	Gyr Z MH	Gyr Z ML	Gyr Z L
Controller	CAN Test	1	1 00001 XXXXX	1	LED on/off							
Controller	Configuration	2	1 00011 XXXXX	1	Config instr							

Figure 2.6: CAN message definition.

2.3 Software Design

Several software items have been designed for the different elements and parts of the MSAS. The sensor element software has been developed with *C++* on the “Atmel Studio” platform. The array controller software has been developed using Python and *C++* for the RaspberryPi 3 version, while Arduino code and *C++* have been used for the Arduino DUE version. The software for the CAN2SPI unit has been developed with “Atmel studio” in *C++*, similarly to the sensor element. The data parsing, mapping, and conditioning as well as the data analysis has been implemented in MATLAB.

2.3.1 Sensor Element

The sensor element software contains an event-driven finite state machine. There are five interrupts that can trigger the finite state machine into a specific state, while a sixth interrupt only resets an internal counter. A simplified description of the sensor element state machine can be found in Figure 2.7.

The sensor element microprocessor has six different interrupt routines. Their name and purpose are briefly described in the following:

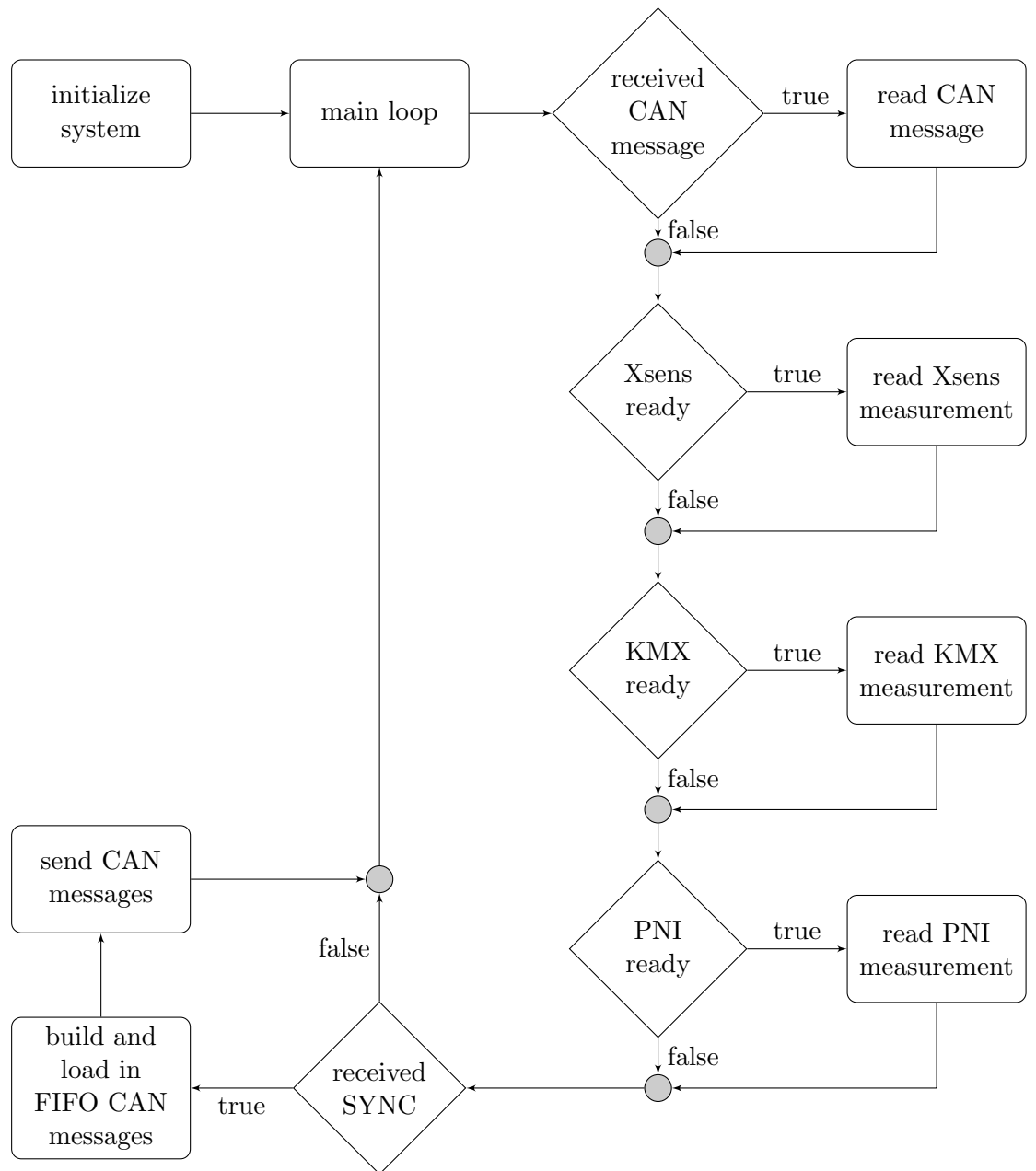


Figure 2.7: Sensor element finite state machine.

- received CAN message
- KMX data ready:
- PNI data ready
- Xsens data ready (when IMU is present)
- SYNC received
- RST received

The first five interrupts trigger interrupt routine in the micro-controller which simply set the corresponding boolean value to *True*; For sake of simplicity, this boolean value has the same name of the corresponding decision cell in 2.7. The last interrupts resets to zero the CAN message counter.

Considering the finite state machine, there are eight different possible states:

- **Initialization:** At power-up, the system is initialized. At first, the configuration parameters written in the EEPROM are read, including CAN address and operating mode. After this step, the CAN unit, the interrupts, the I^2C bus, the message buffer are initialized, and eventually the interrupt reception is enabled.
- **Main loop:** The never-ending loop where the sensor element enters after initialization. It is worth noticing that, in order to have the interrupt routines as light as possible, the effect of an interrupt is often applied when the main loop polls the corresponding boolean flag.
- **Read CAN message:** When a CAN message is received by the sensor element, it is copied to a local buffer and the corresponding flag is set. When in this state, the message is decoded and its instruction is executed: if this is a configuration message, it may require EEPROM writing and reading.
- **Read sensor measurement:** In this state, an I^2C communication is initiated, according to the communication protocol suggested in the relative sensor datasheet, in order to retrieve to sensor measurement. Its time duration varies according to the sensor. During this communication, all interrupts are disabled.
- **Build CAN messages:** When the SYNC interrupt is processed, the micro-controller takes the latest sensor data and build the corresponding CAN messages, as they have been defined in table 2.6. When a message is ready, it is loaded into a FIFO memory, where all CAN messages are buffered waiting to be sent. The Sensor element will send all the elements in the FIFO queue before returning to the beginning of the main loop.

2.3.2 Array Controller

The Arduino DUE array controller has been the only version actually used for the calibration and the experiments. Therefore, the Arduino DUE software only is described in the following Section.

The array controller software is divided between the Arduino DUE board and the CAN2SPI unit. However, the array controller can be described as a unique subsystem. The array controller software consists of a finite state machine, which is graphically represented in Figure 2.8.

Further into detail, there are two interrupts within the unit software, but they are used for internal communication (SPI transmission begin and execution) and therefore do not appear in the finite state machine.

Conversely to the sensor element unit, in the array controller the CAN reception is checked with a polling approach.

In the Arduino DUE array controller, SYNC and RST signals are automatically generated by the u-blox GNSS unit. Additional RST event can be manually triggered by the array controller. Considering the finite state machine, there are eight different possible states:

- **Initialization:** At power-up, the system is initialized. The CAN unit, the interrupts, the SPI bus, the message buffer are initialized, and finally the interrupt reception is enabled.
- **Listen on CAN bus:** This is the main state of the array controller finite state machine. This state is kept until a full data transmission is completed over the array. In the real implementation, the CAN2SPI board is always listening on the CAN bus: the received messages are saved in temporary buffers and retrieved when in this state. This feature insures that no message is lost while the other software states occur.
- **Internal SPI transmission:** When all the 35 CAN messages are received and buffered in the CAN2SPI unit, a signal is raised to notify the Arduino DUE board. This event starts the SPI communication between the two sub-units, which ends after all the messages have been delivered. Afterwards, the CAN2SPI board buffer is cleared.
- **Send messages to computer:** The CAN messages, with address and payload, are retrieved by the Arduino DUE through the SPI bus and forwarded to the computer over a USB connection.
- **Generate RST signal:** The Arduino DUE can receive over the serial interface the instruction to trigger a RST event, i.e. to set to zero all the CAN message counters in all sensor elements. The signal is generated locally and hardware converted to a differential signal.

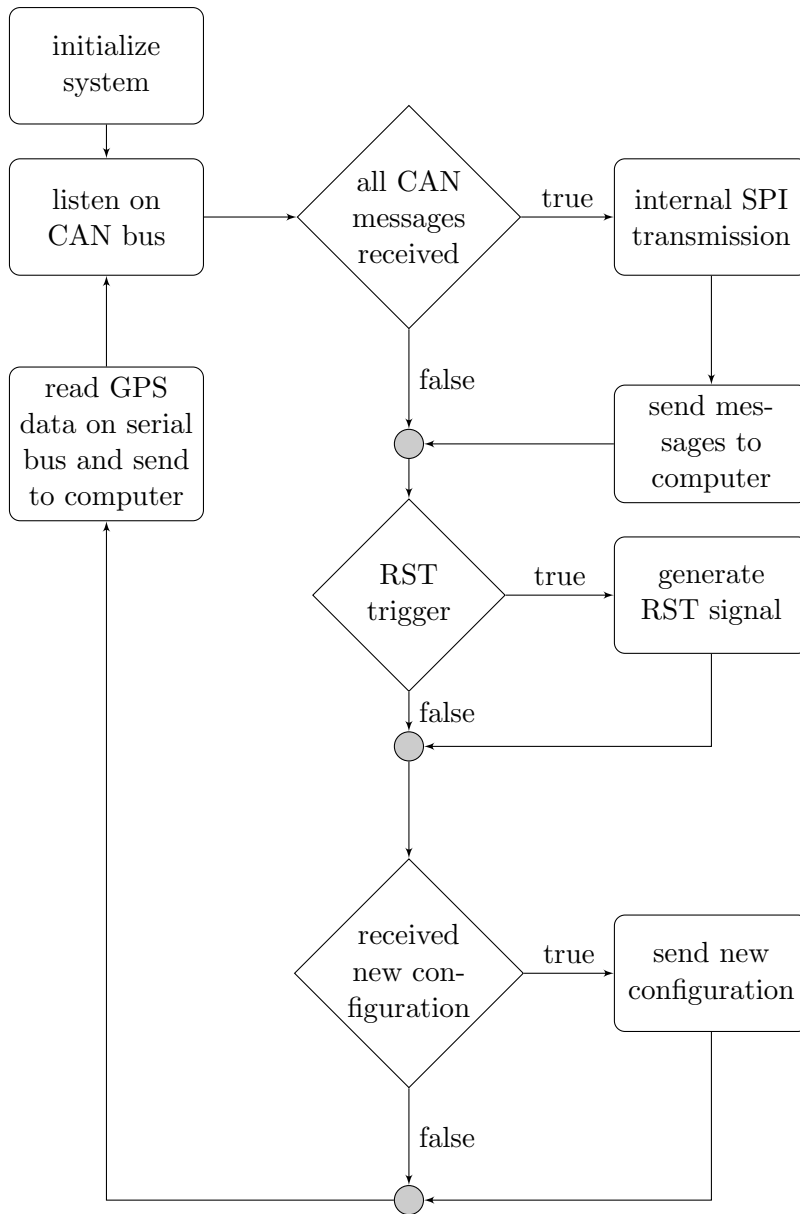


Figure 2.8: Array controller finite state machine.

- **Send new configuration:** The sensor element configuration can be modified in software from the computer to which the array controller is connected. When a new configuration message is received by the array controller, an SPI transmission is performed towards the CAN2SPI board, where a CAN message containing the configuration instructions is generated and sent along the CAN bus.
- **Read GPS data:** Every second a GPS data message is delivered on the serial bus from the GNSS unit to the Arduino DUE. when the message is received, it is forwarded to the computer on the USB link.

2.3.3 Data Processing

The data stream from the array controller to the computer consists of magnetic measurements and NMEA [17] messages. The MATLAB software receives this data stream over the serial port and saves the received data to a CSV file. The data processing and analysis is carried in post-processing.

The very first operation is to separate the magnetic measurements from the NMEA messages. Temporary GNSS non-availability is handled in this phase.

The second operation is to separate the single magnetic measurements from one another. At this stage the measurements are still embedded in the CAN message format, that contains the sender address and the message counter too. The sender address is necessary to distinguish among the sensor element and magnetic sensor type; the message counter is needed to attribute an accurate timestamp to the magnetic measurement.

The third step is to recognize the CAN addresses saved in the messages. When all CAN addresses have been identified, the messages are separated by sensor and the magnetic measurement is reconstructed for all magnetic sensors in the array. Each measurement is also provided with an absolute and relative timestamp and (when available) with the geographical coordinates at the sampling instant. Eventually, all the magnetic measurements are scaled with the computed calibration coefficients (see Chapter 3).

At this point the data is calibrated and geo-referenced. However, the target magnetic signature is function of the space: a conversion from time domain to space domain is therefore needed. The distance between the measurements at the sampling time is computed using the GNSS *Speed Over Ground* (SOG) information. Finally, the space signal is re-sampled so to have a measurement every 10 cm. The obtained signal is then filtered with a band-pass filter in the spacial domain, to retain only the spacial frequencies relevant for the train localization evaluation. A graphical representation of the frequencies of interest is shown in Figure 2.9. The target signals have

spacial period in the interval $[5,25]$ meters, which is equivalent (for train speed up to 200 km/h) to a time frequency interval of $]0, 11]$ Hz.

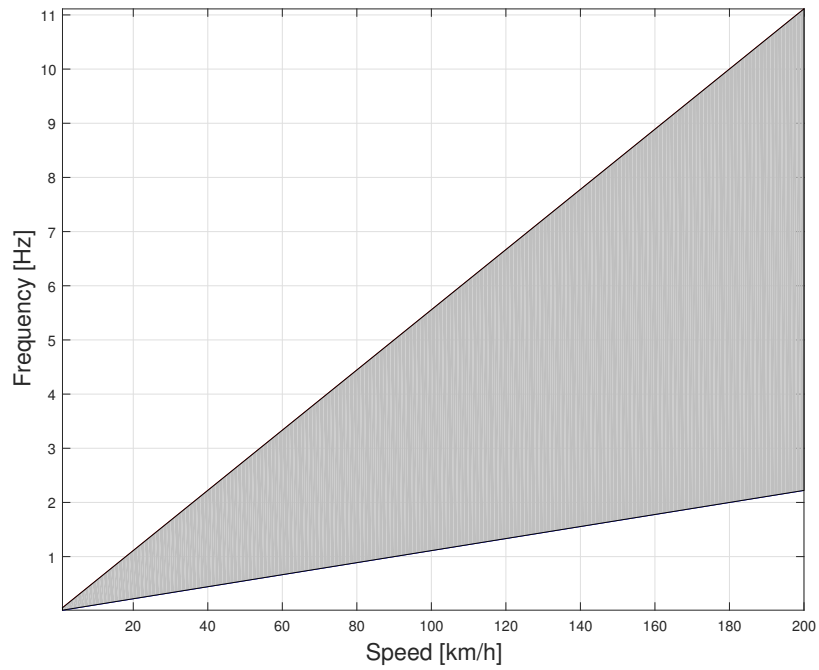


Figure 2.9: Target magnetic signal frequencies as a function of the train velocity. The relevant frequencies are within the gray area of the plot.

Chapter 3

Calibration

Both magnetic sensor datasheets (KMX and PNI) give no information about sensor calibration. However, multiple preliminary data recordings shed light on two facts: first, a rough factory calibration had been performed; second, this calibration was not accurate enough for the MSAS purposes. A further calibration was therefore necessary to get reliable data from the MSAS.

Constant Earth's magnetic field was assumed for the calibration, i.e. the Earth's magnetic field intensity is considered constant over the whole MSAS. The reference sensor (see 2.2.1) is used in this procedure. The reference sensor measurements are considered the real value for the local magnetic field intensity: no further distinction between real magnetic field intensity and reference measurements will be considered in the following.

3.1 Calibration Method

3.1.1 Magnetic Field Measurement Model

Considering a generic magnetic sensor, its measurement \underline{m}_{sensor} differs from the real magnetic field \underline{m}_{real} by the related measuring error $\underline{\nu}$:

$$\underline{m}_{real} = \underline{m}_{sensor} + \underline{\nu}. \quad (3.1)$$

The measurements \underline{m}_{real} , \underline{m}_{sensor} and $\underline{\nu}$ are column vectors of size $[3 \times 1]$, that contains a component for each spatial dimension.

Considering the environment in which the MSAS operates, and the previous related works [3, 4], the magnetic field components are modeled as constant and linear. The higher order components are neglected and considered as noise.

Accordingly to this assumption, the model for magnetic field measurements is:

$$\underline{m}_{real} = \underline{A} \cdot \underline{m}_{sensor} + \underline{b} + \underline{n}, \quad (3.2)$$

or in explicit form

$$\begin{bmatrix} m_{r,1} \\ m_{r,2} \\ m_{r,3} \end{bmatrix} = \begin{bmatrix} a_1 & a_2 & a_3 \\ a_4 & a_5 & a_6 \\ a_7 & a_8 & a_9 \end{bmatrix} \cdot \begin{bmatrix} m_{s,1} \\ m_{s,2} \\ m_{s,3} \end{bmatrix} + \begin{bmatrix} b_1 \\ b_2 \\ b_3 \end{bmatrix} + \begin{bmatrix} n_1 \\ n_2 \\ n_3 \end{bmatrix}. \quad (3.3)$$

In equation 3.2, matrix $\underline{\underline{A}}$ is the linear parameter matrix for axis scaling factors and cross-axis relation. For a perfectly calibrated measuring system, $\underline{\underline{A}}_{ideal}$ is:

$$\underline{\underline{A}}_{ideal} = \begin{bmatrix} 1 & 0 & 0 \\ 0 & 1 & 0 \\ 0 & 0 & 1 \end{bmatrix}. \quad (3.4)$$

The offset vector \underline{b} of equation 3.2 is the constant component of the measuring error of equation 3.1.; Finally, \underline{n} is the noise residual component. As there is no further knowledge on the noise characteristics, it is considered as additive white Gaussian noise.

3.1.2 Evaluation of Calibration Parameters

According to the measurement model presented in Section 3.1.1, $\underline{\underline{A}}$ and \underline{b} components are needed in order to perform the conversion from measured to real magnetic field. These 12 parameters are evaluated using the mean squared error minimization algorithm for regression, starting from a dataset for which the real value of the magnetic field is known.

Starting from equation 3.2, the measuring model is reshaped in a more compact form, where the real magnetic field vector is obtained with a single algebraic multiplication:

$$\underline{m}_{real} = \underline{\underline{\tilde{M}}}(m) \cdot \underline{\theta} + \underline{n}, \quad (3.5)$$

or in explicit form :

$$\begin{bmatrix} m_{r,1} \\ m_{r,2} \\ m_{r,3} \end{bmatrix} = \begin{bmatrix} m_1 & m_2 & m_3 & 0 & 0 & 0 & 0 & 0 & 0 & 0 & 1 & 0 & 0 \\ 0 & 0 & 0 & m_1 & m_2 & m_3 & 0 & 0 & 0 & 0 & 0 & 1 & 0 \\ 0 & 0 & 0 & 0 & 0 & 0 & m_1 & m_2 & m_3 & 0 & 0 & 0 & 1 \end{bmatrix} \cdot \begin{bmatrix} a_1 \\ a_2 \\ \vdots \\ \vdots \\ a_9 \\ b_1 \\ b_2 \\ b_3 \end{bmatrix} + \begin{bmatrix} n_1 \\ n_2 \\ n_3 \end{bmatrix}. \quad (3.6)$$

where $\underline{\theta}$ is the $[12 \times 1]$ column vector with all the linear and constant parameters, and $\underline{\underline{\tilde{M}}}(m)$ is the measurement matrix, shaped so that, considering equation 3.5 and 3.2:

$$\underline{\underline{\tilde{M}}}(m) \cdot \underline{\theta} = \underline{\underline{A}} \cdot m_{sensor} + \underline{b}. \quad (3.7)$$

Referring to equation 3.5, the aim is to estimate the $\underline{\theta}$ vector. Therefore the pseudo-inverse of the $\underline{\tilde{M}}(m)$ is computed:

$$[(\underline{\tilde{M}}^T \underline{\tilde{M}})^{-1} \underline{\tilde{M}}^T] \cdot \underline{m}_{real} = \underline{\theta}. \quad (3.8)$$

Considering N measurements, in equation 3.8 the $\underline{\tilde{M}}$ matrix has dimension $[3 \times N, 12]$. Likewise, \underline{m}_{real} has dimension $[3N \times 1]$.

In order to estimate all the model parameters, multiple magnetic measurements are required: in absence of noise, 4 independent measurements on all three axis would be enough to resolve the linear system, while in a realistic case, the parameter estimation improves by increasing the considered measurement number.

3.2 Calibration Setup



Figure 3.1: MSAS calibration setup.

The calibration setup is shown in Figure 3.1. It is designed in order to minimize its own magnetic influence on the measuring system: the array is lifted from the ground using a wooden tripod and aluminum carabiners and nylon ropes, all of which are non-ferromagnetic materials. Furthermore, the calibration is performed in open fields, far away from metallic structures or

building that could affected the magnetic measurements and invalidate the assumption of constant magnetic field state above.

The reference sensor is fixed on the MSAS itself, close to its center.

A set of static measurements was performed, placing the MSAS in a different spatial orientation at each measurement. The sensor measurements are averaged over 100 readings, to filter out measurement noise from the sensor readings. The reference sensor measurement, instead, is taken as single, given its superior accuracy and for sake of simplicity.

Eventually, 42 static measurements were performed.

The euclidean norm of each 3D sensor measurement should be equal to the local Earth magnetic field: this is the direct consequence of the initial assumption of constant magnetic field. The single axis components, instead, vary according to the sensor spatial orientation. The model presented in Section 3.1.1 is applied in order to evaluate equation 3.8. Here, all performed measurements are considered at a time. The obtained parameter vector, with both linear and offset parameters, is then stored in the MSAS data analysis software, and it is not directly applied to the physical sensor. The calibration parameters are applied in software to the raw data retrieved from the MSAS at every use.

The parameter vector is unique for each one of the 22 magnetic sensors present in the MSAS and, of course, evaluated independently.

3.3 Results and Discussion

The obtained results proved the existence of a previous factory calibration for both the PNI and the KMX sensor: The obtained linear parameter matrix (refer to Section 3.1.1 for further details) was, for all sensors, in the range of ± 0.05 from the ideal identity matrix. Conversely, the offset vector has considerable importance, especially for the KMX sensors. The comparison between the sensor measurements before and after the calibration is shown in Figure 3.2: each line represents one sensor measurements, along all the calibration measurement set.

The reference sensor as expected has a quasi-constant measurement set at about $48 \mu\text{T}$. Before the calibration, the PNI sensors are in a range of $\pm 4.6 \mu\text{T}$ from the real value, while the KMX sensors are in a range of $\pm 112 \mu\text{T}$ from the real value. After the calibration is performed, for the same measurement set we have the PNI and the KMX sensors respectively at $\pm 1.8 \mu\text{T}$ and $\pm 2.9 \mu\text{T}$ from the true magnetic field intensity measured by the reference sensor.

To validate the calibration, a double evaluation has been performed. The first is to compute the error between the calibrated measurement and the real

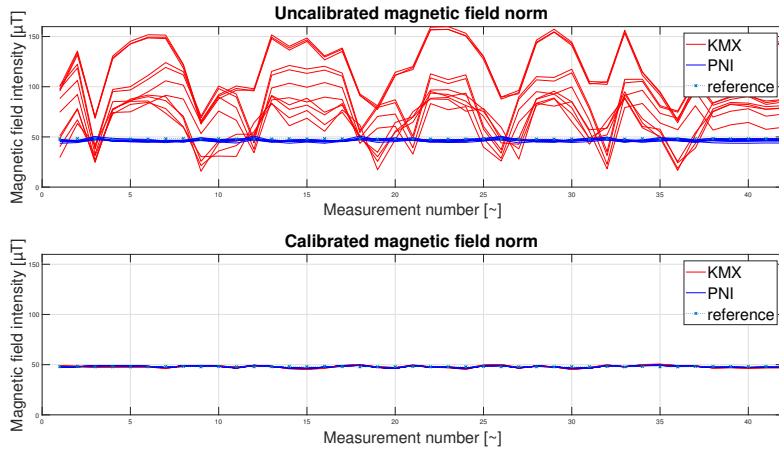


Figure 3.2: Measured magnetic field norm comparison, before and after calibration.

Considered measurements	Max error [μT]
3	60.39
4	6.80
5	5.52
11	4.80
14	3.53
34	2.95
41	2.87
42	2.86

Table 3.1: Relation between considered calibration measurements and measurement error.

magnetic field relatively to the target signal. The MSAS aims at measuring magnetic field variation greater or equal to $\pm 3 \mu\text{T}$, according to [4]. The PNI sensor is widely within the required accuracy threshold, while the KMX is closer to the limit.

The second is to investigate how the maximum calibration error changes with increasing number of considered measures.

Table 3.1 shows that the measurement error decreases when considering more calibration measurements. Nevertheless, an asymptotic behavior is reached when considering more than 30 measurements: this residual error might be caused by measurement noise or non linear components, which are considered as noise in the measuring model (section 3.1.1). This analysis shows that the residual errors in the calibration parameters are not the limiting factor for the MSAS accuracy.

Chapter 4

Magnetic Localization

This experiment aims to answer the first two questions driving the work of thesis. The first question is if low-cost magnetic sensors can achieve the same level of train localization accuracy that the high-cost sensor reached in [4]. The second objective of this experiment is to understand if multiple sensor along the cross-track direction are useful to improve train localization accuracy.

The experimental setup is in the automotive environment, with the MSAS placed behind the road vehicle. The test presented in the following was the first of its genre and many practical issues had to be solved in order to perform the experiment. Future related works may address magnetic signature localization in a railway environment. Despite the difference between automotive and railway environment, the results obtained from this experiment showed that the actual measured variations in the magnetic field are comparable to the ones found in literature [2, 3]. An additional argument has to be considered: a car has more spacial degrees of freedom than a train: a car passing multiple times over the same path does not reproduce exactly the same journey. It is reasonable to assume that achieving accurate magnetic localization is more difficult in automotive than in railway environment, and that the results obtained from this experiment are relevant for the railway environment too.

4.1 Experimental setup

The sensor array was placed centered and behind the test vehicle. The array controller was inside the vehicle, powered by an external 12 V battery. The array controller was also connected to the commercial GNSS module, with the receiving antenna placed on the top of the vehicle. A laptop was used to issue the instructions and retrieve the magnetic and GNSS data from the array controller.

The measuring phase took place inside the DLR facility. The vehicle



Figure 4.1: Experiment setup: The MSAS is placed behind the road vehicle, as far as possible from the electro-magnetic disturbances generated by the car.

went along the same path for 10 runs. The magnetic data have been georeferenced with the GNSS module. The path length is approximately 360 m. Exploiting the GNSS information, the magnetic data was converted from time to spacial domain. Figure 4.2 shows the complete data recorded by the PNI sensors, in the time domain: for all 11 PNI sensor the magnetic field magnitude is plotted. Even at a qualitative level, it is possible to distinguish two characteristics: first, that the magnetic signal of every sensor is periodic; second, that the recorded signal is different from sensor to sensor. The first characteristic is used to derive the magnetic signature of the path, as each signal period stands for a run over the experimental path. The second characteristic means that the recorded magnetic signatures are partially independent from one another. Signature independence is exploited to refine the localization estimation.

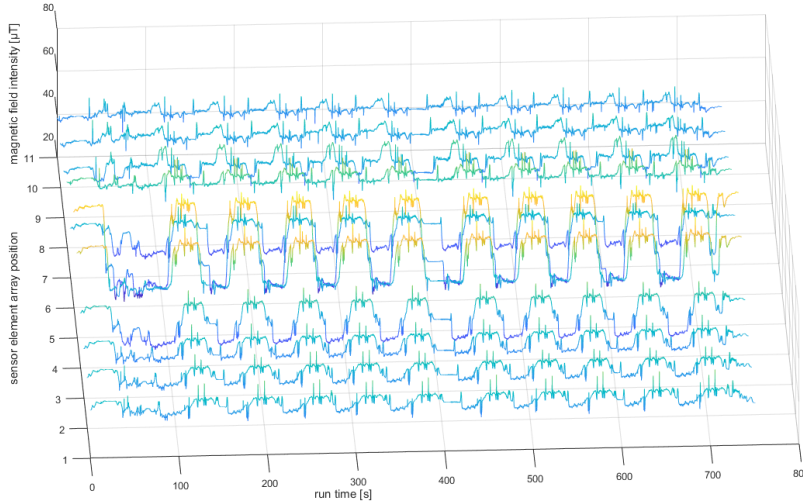


Figure 4.2: Example of array magnetic recording. PNI measurements only are plotted.

4.2 Methods

4.2.1 Data Conversion: from Time to Space Domain

The MSAS records magnetic data at a frequency of 200 Hz, while the GNSS data is retrieved every second. As explained in 2.2.3, the two data flow is perfectly synchronized.

The data is therefore recorded in time domain. Being the magnetic signature a space function, a domain conversion from time to space is needed. For further details refer to section 2.3.3.

The data conversion from time to spacial domain is based on GNSS data. The start and end point of the experimental run are found using geographical coordinates. The starting point of each run is the 0 m relative position. The intermediate points are converted thanks to the SOG value taken from the GNSS data. The magnetic data, now function of a uni-dimensional spatial variable, are re-sampled every 10 cm. Figure 4.3 shows the superposition of the magnetic data relative to the 10 runs in spacial domain, for the MSAS right-most PNI sensor. It is possible to notice that most runs have the same behavior, while sometimes appreciable perturbation occurs out of the main pattern. Some perturbation are most likely due to other vehicles passing by the MSAS, some are due to the slight position changes in the cross-velocity direction.

The magnetic data from the sensors have been filtered, as explained in section 2.3.3, in order to keep only the relevant signal dynamics, excluding all constant and higher frequencies components, which are not related to the

magnetic signature.

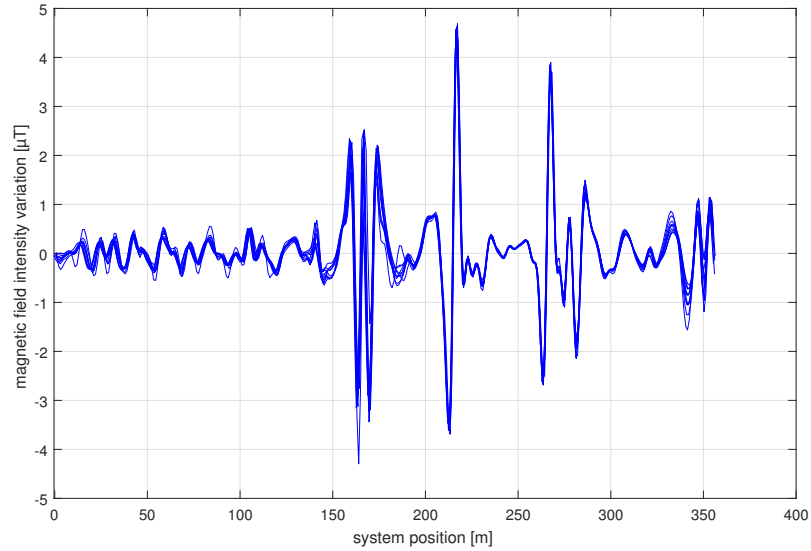


Figure 4.3: Superposition of multiple magnetic signatures of the same path.

During the first run along the path, no other vehicle passed close to the MSAS, thus providing a good magnetic signature. For all sensors, the first run along the chosen path was selected as the reference magnetic signature. The magnetic position estimation is obtained looking for the best match between the reference signature and the considered signature previous to the estimated point. The length of the compared signature is one of the system variables: the longer the magnetic signature section, the lower the localization error. On the other hand, longer magnetic signature sections require higher computational power.

4.2.2 Position Estimation Methods

Two main methods have been applied to perform the position estimation: cross-correlation and L_1 signal difference. The position estimation is referred in the following as P_{est} .

Cross-correlation

The first applied method for signal comparison is cross-correlation [18]. Given two finite, real and discrete signals f and g , the cross-correlation of the two is defined as:

$$(f * g)[n] = \sum_{n=-(N-1)}^{N-1} f[n]g[n+d], \quad (4.1)$$

where the index d is the displacement between the signals with respect to the reference frame and n is the maximum signal length. The cross-correlation provides a measure of the similarity of the signals, but it is influenced by the signal amplitude. If the signal amplitude is not constant, the parts with greater amplitude have a large impact on the cross-correlation result. This characteristic leads to ignore the dynamics of the signals with smaller amplitude, which are not less valuable for the signal matching.

Cross-correlation can alternatively be computed using the Fourier transform or the Fast Fourier Transform (FFT) method, with large computational cost saving. The cross-correlation of the two signals is therefore obtained as:

$$(f * g) = \mathcal{F}^{-1}\{\mathcal{F}\{f * g\}\} = \mathcal{F}^{-1}\{\overline{\mathcal{F}\{f\}} \cdot \mathcal{F}\{g\}\}. \quad (4.2)$$

L_1 signal difference method

The second applied method is the L_1 signal difference, also known as L_1 norm or Manhattan difference [19]. This method is here referred as L_1 . Given two discrete signals f and g , L_1 is defined as:

$$\left\|L_1(f, g)[n]\right\| = \sum_{n=-(N-1)}^{N-1} \left|f[n] - g[n+d]\right|. \quad (4.3)$$

The indexes are the same as defined for equation 4.1. The difference of the two signals gives a measure of the two signal relative behaviour [20]. Where the difference is minimum, the signals are the most similar. L_1 method is able to distinguish when two signals have similar behavior but different amplitude and performs better than cross correlation on this work target signals of this work.

Combining data of multiple sensors

The MSAS measures with eleven sensor elements. Each one of the sensor elements is equipped with two magnetic sensors, the KMX and the PNI. In order to provide comparison between the two sensor performances, the KMX and the PNI sensors have been considered separately in the following.

Considering cross-correlation, four different methods have been applied to combine the data from multiple sensors [21]. The first method is to sum all the cross-correlation score vector:

$$P_{est} = \max \left(\sum_{n=1}^{11} (s_{ref} * s_n) \right), \quad (4.4)$$

where s_{ref} is the reference magnetic signature and s_n is the magnetic signature recorded by sensor n . By summing all the cross-correlations scores, the peak corresponding to the true position estimation is summed iteratively. Similarly all the noise peaks are summed to one another and are therefore averaged.

The second method considers a position estimate from the sensor that has the highest cross-correlation peak:

$$P_{est} = \max_{n \in [1,11]} \left(\max (s_{ref} * s_n) \right), n \in N. \quad (4.5)$$

This method aims to exclude all sensors which could not achieve a safe position estimation and therefore have multiple peaks all in the same range. The liability of this method is that signal amplitude is not constant, and therefore noisy peaks might theoretically have high cross-correlation scores.

The third method computes the median of the position estimation obtained by all sensors:

$$P_{est} = \text{median} \left(\max (s_{ref} * s_n) \right), n \in N. \quad (4.6)$$

This method contains a compromise choice, avoiding maximum and minimum estimated values. If six or more sensors make a correct estimation, this method provides for sure an accurate position estimation.

The last applied method is similar to (3), but here the mode is considered: The position estimation is therefore the value obtained by most of the sensors:

$$P_{est} = \text{mode} \left(\max (s_{ref} * s_n) \right), n \in N. \quad (4.7)$$

This method performs better in moderate noise scenario, where just a few sensors can point to the correct value, while it performs as the median when most sensors perform the same estimation. If all sensor provide different position estimation, the mode method returns the one closest to the starting point.

Considering the L_1 method, the multiple sensor data where combined exploiting two different method, the median and the mode one. Similarly to equation 4.8 and 4.9, for L_1 the median method can be written as:

$$P_{est} = median\left(\max\left\|\left|L_1(f, g)[n]\right|\right\|, n \in N, \right) \quad (4.8)$$

while the mode method can be written as:

$$P_{est} = mode\left(\max\left\|\left|L_1(f, g)[n]\right|\right\|, n \in N. \right) \quad (4.9)$$

The same considerations done in the cross-correlation section hold here for both method.

4.2.3 Evaluation of Localization Accuracy

For all recorded signatures but the reference one, 100 positions are estimated through magnetic localization and compared to the true value. If the error of the estimated position falls within the defined threshold, the estimation is considered as correct. The chosen thresholds for the correct localization assessment are 4 m and 2.5 m of error, which are standard values for user range error and accurate localization in GPS positioning [22, 23]. The GNSS position estimation is taken as true value. All GNSS estimated positions have been verified to have errors smaller than 1 m, which is a acceptable error for this experiment purposes.

4.3 Results and Discussion

The magnetic localization performances have been evaluated both for the KMX and for the PNI sensors. The PNIs performed slightly better than the KMX sensors, but the applied localization methods have similar behaviors for both sensors. To avoid repetitions, the methods performance comparison is discussed for the PNI sensor only. The performance comparison between PNI and KMX can be found in section 4.3.2.

4.3.1 Methods' Performance and Comparison

The different methods presented in section 4.2.2 are showed and discussed in three different ways. The first approach is to show the localization error for all estimated positions and all different runs, as a function of the space: here, qualitative considerations can be made upon the various methods.

The second approach is, for all methods, to show the accuracy performance as a function of the considered signature length used for best match evaluation: here, quantitative considerations are made about the performance level of each method.

The third approach shows the accuracy performances as a function of the

considered error threshold: here, the maximum localization errors and their probability are shown.

Figure 4.3 shows the magnetic signature dynamic along the considered path: the signal amplitude is extremely variable. The cross-correlation method is based on signal product: with a signal with large amplitude shifts, the highest cross-correlation scores are most likely evaluated for the point with maximum amplitude. For this reason, all cross-correlation methods have poor performances regarding magnetic localization.

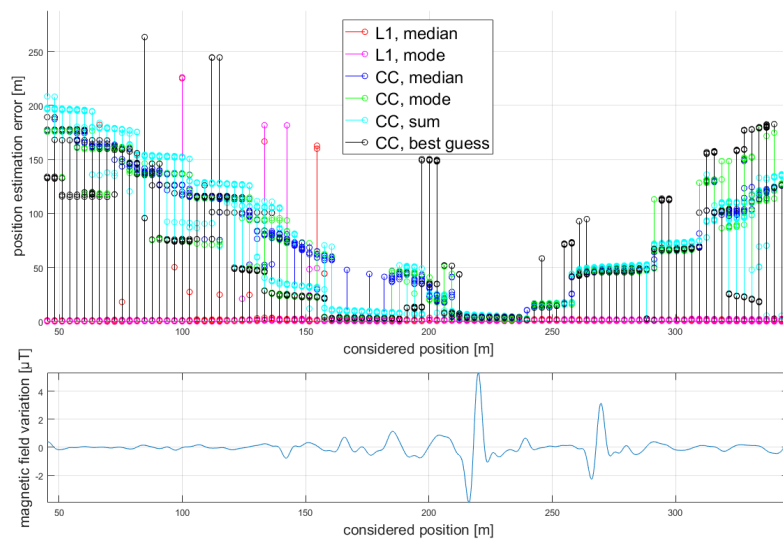


Figure 4.4: Magnetic localization error for 100 different path positions. The compared signature is the section of 25 m previous the estimated position. The lower part of the figure shows the reference signature for the first PNI sensor. Localization is estimated matching the last 25 m of recorded signature to the reference signature.

Figure 4.4 shows the localization error for the six discussed methods that consider multiple sensor data. The cross-correlation error is proportional to the distance between the considered position and the highest signature peak. On the contrary, The *L1* method has surprisingly high accuracy performances: three out of nine runs have maximum localization error smaller than 2.5 m. Considering 2.5 m as the error threshold, the overall accuracy is above 95% for both KMX and PNI sensors, considering both median and mode methods.

In total, the accuracy performances of eight different methods have been evaluated. The result is shown in figure 4.5. This plot shows the correct localization estimation within 2.5 m over different signature lengths. A substantial performance gap separates the cross-correlation methods from

the $L1$ methods. Considering the $L1$ method and a comparison signature of 25 m, the single sensor localization reaches accuracy higher than 80%, which is a remarkable result when compared to all cross-correlation methods. Considering multiple sensor data, the best performing method is the mode, which reaches accuracy of 96% for considered signature of 25 m and even accuracy higher than 99% for considered signature of 30 m. The median method has slightly worse performances for shorter considered signatures, eventually reaching the mode accuracy performances for signatures longer than 30 m.

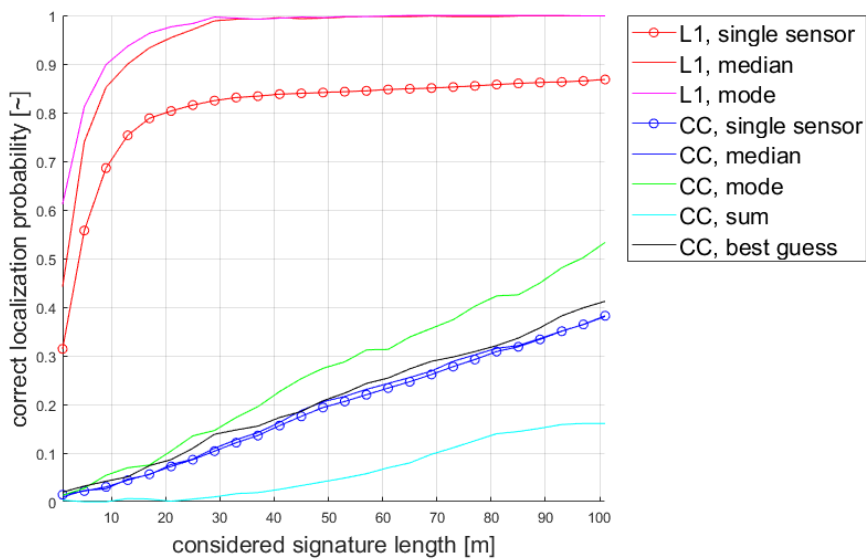


Figure 4.5: Magnetic localization performances for all evaluated methods. The plot shows the correct estimation probability as a function of the considered signature length. The threshold for correct estimation is set at maximum error equal to 2.5 m.

About the cross-correlation methods, best results are obtained for the mode method. Anyway, the performance accuracy is poor enough to suggest to exclude all cross-correlation methods from further research developments in the field. In addition to this, it is worth noticing that even the linear improvement in the cross-correlation methods' performance is misleading: increasing the considered signature length means that the estimated positions are shifted more to the final part of the experimental path, therefore linearly increasing the number of estimations where the maximum signature peak is considered.

Finally, figure 4.6 shows the probability of correct magnetic localization as a function of the considered error threshold. The considered signature length is 25 m. As expected, the $L1$ methods have overwhelming performances with respect to all cross-correlation methods. In particular, for the single sensor

L1 method, 90% of all position estimations are within 15 m of error from the GNSS value. Considering a combined sensor approach, nearly 99% of the position evaluations are within a 6 m error threshold. Again, the cross-correlation methods have very poor performances: only 50% of the estimated position have an error smaller than 45 m, for the best performing method. It is therefore safe to state that the cross-correlation methods are highly inaccurate when performing magnetic localization.

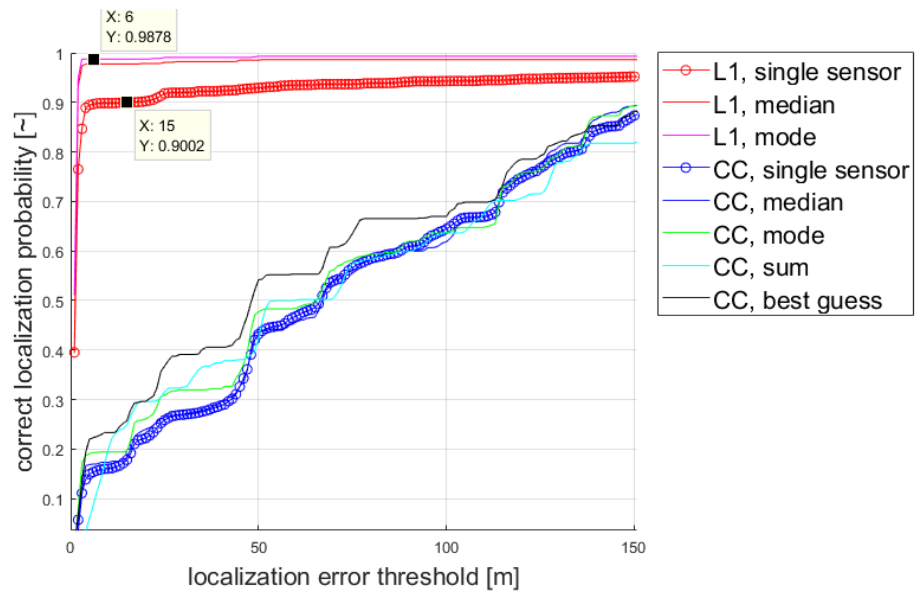


Figure 4.6: Magnetic localization performances for all evaluated methods. The plot shows the correct estimation probability as a function of the considered error threshold. The magnetic signature length considered for Localization estimation is 25 m.

4.3.2 Performance Comparison of PNI and KMX sensors

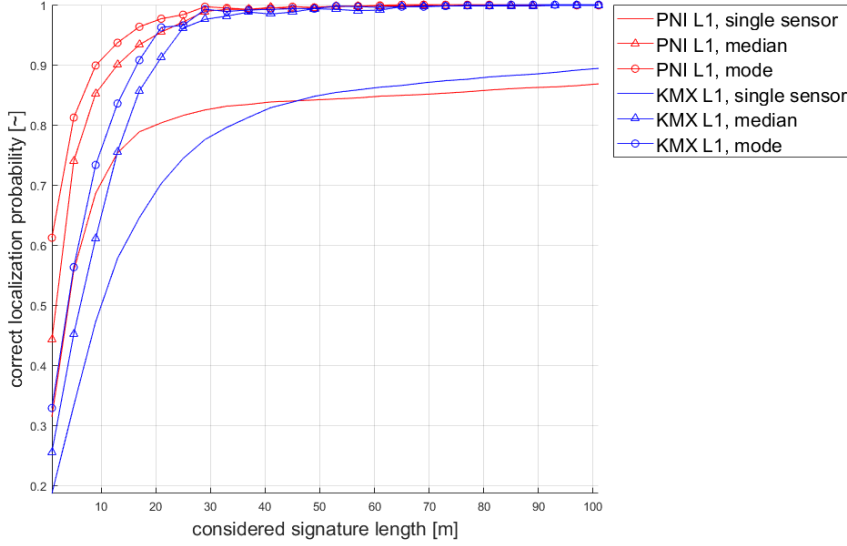


Figure 4.7: Magnetic localization performances for PNI and KMX sensors. Only the $L1$ methods are reported. The plot shows the correct estimation probability as a function of the considered signature length. The threshold for correct estimation is set at maximum error equal to 2.5 m.

The magnetic data retrieved from the MSAS are either from the PNI sensor or from the KMX sensor, which are presented in detail in section 2.2.1. During the experiments, the sensor data have been treated separately for sensor type, as if they were from two different measurement system. This procedure now allows to draw conclusion about the sensor performances and help in deciding the next steps in the research. As the cross-correlation methods proved to be inaccurate for magnetic localization, they are not reported in the comparison analysis. Figure 4.7 shows the localization performances for both sensor types: when multiple sensor data are combined, PNI sensor have a slightly better performance, especially when short signature are compared. On the single sensor performance, however, for longer compared signatures the KMX sensor provides better performances. This behaviour, quite unexpected, might be due to the experimental setup: as the considered path is only 360 m long, considering long signatures for comparison might lead to numerical errors. In any case, when an error threshold of 4 m is considered, PNI sensor always perform better than the KMX, especially on short compared signatures. The comparison with error threshold at 4 m is shown in figure 4.8. The overall behaviour of the different methods, however, is unchanged.

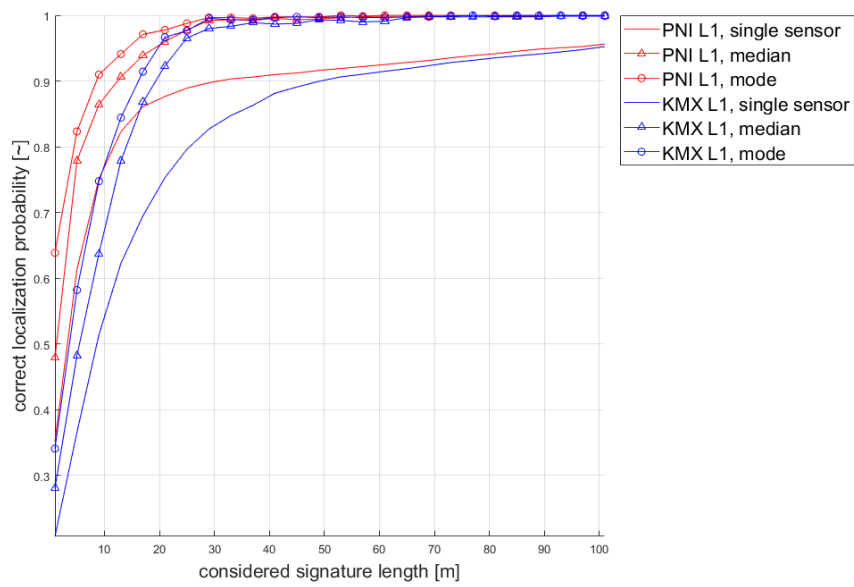


Figure 4.8: Magnetic localization performances for PNI and KMX sensors. only the $L1$ methods are reported. The plot shows the correct estimation probability as a function of the considered signature length. The threshold for correct estimation is set at maximum error equal to 4 m.

Chapter 5

Neighboring Train Disturbance Analysis

One of the main problems in magnetic localization [2] is that a strong magnetic perturbation, such as a train passing on a parallel track, temporarily interferes with the system, preventing accurate magnetic localization. The objective here is to understand if a multiple sensor system such as the MSAS, with sensors from one train side to the other, is beneficial in a detection of this interference. This experiment addresses the third question of this work of thesis: to understand if a neighboring train can be recognized when approaching the MSAS and if its magnetic disturbance can be excluded when estimating the system position.

The MSAS is static during the data collection phase. The experiment presented here cannot inquire if the localization accuracy is influenced by a neighboring train, because the MSAS was not mounted on a train. Instead, this experiment focuses on a neighboring train identification using the magnetic data and on determining how fast the train magnetic influence fades along the cross-track direction.

5.1 Experimental Setup

The experiment took place on the platform of the train station in Weßling. As shown in Figure 5.1, This station has a central platform, with railway tracks both on the left and on the right side. The MSAS was laid on the ground perpendicular to the platform, placed approximately at the same distance from the two tracks. The MSAS was placed in a position that is compatible with an additional track between the existing two: This setup provides realistic information about the distortion that a train equipped with the MSAS would experience from a train passing on a parallel track. In numbers, the center of the MSAS was placed at 3.5 m from both track centers. The actual distance between the train side and the sensor element

was in the range of 1.15 to 3.15 m.

Figure 5.1 shows the experimental setup. The sensor X-axis is aligned with the track direction and the cable direction. Thus, the magnetic perturbation caused by the currents flowing in the cables should theoretically be undetectable on the X-axis.

The MSAS is connected to a laptop, which stored the real time data flow. The record time was 25 minutes, and it allowed to record four train transits. Train 1 and 2 passed on the MSAS side at low speed, while train 3 and 4 actually stopped in front of the system for a few seconds. Besides, train 1,2, and 4 passed close to the sensor element 11 of the MSAS, while train 3 passed close to sensor element 1. The data analysis was performed after the end of the data collection phase.



Figure 5.1: Experiment setup: The MSAS is placed on the platform, perpendicular to the train direction of motion and at the same distance from left and right tracks. Sensor element 1 is on the left side of the picture, sensor element 11 is on the right side.

5.2 Methods

As the data collection was static, no time to space conversion is needed in this experiment. The raw data collected during the experiment had strong unexpected disturbances that prevented from identifying the train transits. The magnetic field norm recorded by the MSAS PNI sensors is shown in Figure 5.2. The four time windows where the train transit happened cannot be seen easily in a qualitative way: major disturbances hide the target values of this experiment. Performing a spectral analysis of the recorded signal provides useful information on the signal characteristics: as shown in Figure 5.3, some high-power frequencies have high influence on the final signal shape: The most powerful frequency is at 16 Hz, which is the electric current

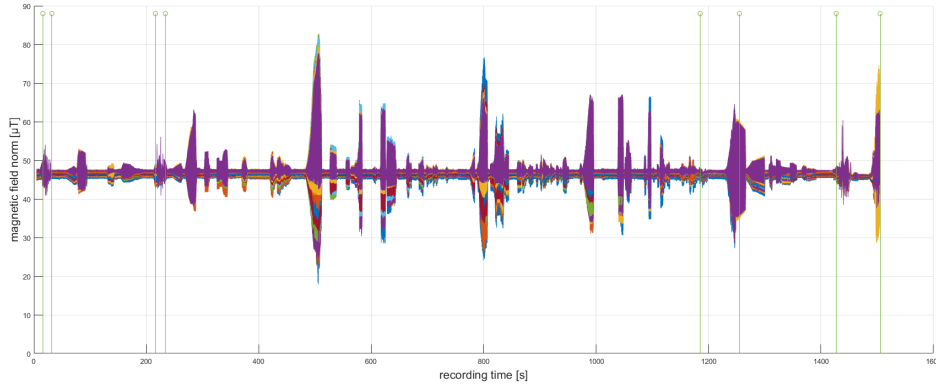


Figure 5.2: Unfiltered magnetic field norm recorded at the train station. The vertical lines identify the actual time windows of train transit. The different colors stand for the multiple PNI sensor data.

frequency in railway environment in Bavaria. The harmonic components of the electric currents can be seen too, for example at 32 Hz and 48 Hz. As the currents flow in cables parallel to the railway track, their induced magnetic field is mostly perpendicular to the track direction. Given the experimental setup, Y and Z axis of the sensor elements are the most influenced by the electric currents flowing over the railway tracks. Their intensity is such that the norm of the maximum magnetic disturbance recorded by the magnetic sensors is larger than $40 \mu\text{T}$, meaning that it is nearly as strong as the Earth's magnetic field. When considering the magnetic field norm, the current components are so wide and complex that filtering them away is difficult. Instead, when only the X-axis is considered, filtering the undesired components becomes feasible.

In this experiment only the magnetic data recorded over the sensor X-axis is considered, in order to reduce the electric current influence. To the raw magnetic data is firstly applied a band-stop filter to eliminate the powerful current components; secondly, a high pass filter is applied to remove static and extremely low components (below 1 Hz). Finally, a low pass filter is applied to remove components over 5 Hz. The result of the filtering phase is shown in Figure 5.4: the disturbance caused by trains 1, 2 and 4 are now clearly visible, while the current components are now negligible when compared to the train signal. Train 3 is hardly visible, which is a positive fact: its transit happens on the opposite side of the MSAS, close to the sensor element 1.

Data filtering is performed using and type II Chebyshev filters[24]. Type I Chebyshev filter was not used because of its ripple in the pass-band close the the cutoff frequency, while the Type II Chebyshev has no ripple in the pass-band, but has ripple in the stop-band. For the Type I filter, the gain

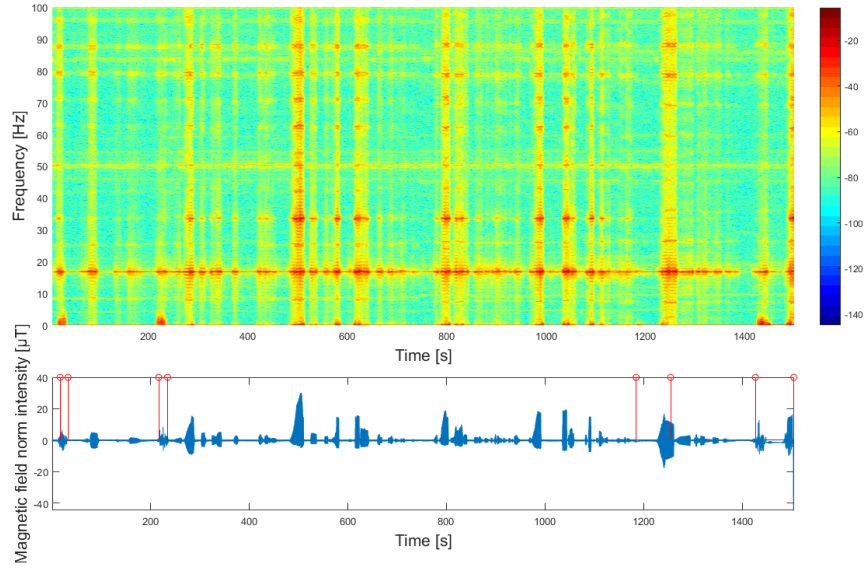


Figure 5.3: Spectral analysis of the PNI sensor in sensor element 11. Original unfiltered data on X-axis. The disturbances generated by the train passage are invisible because of the current disturbances.

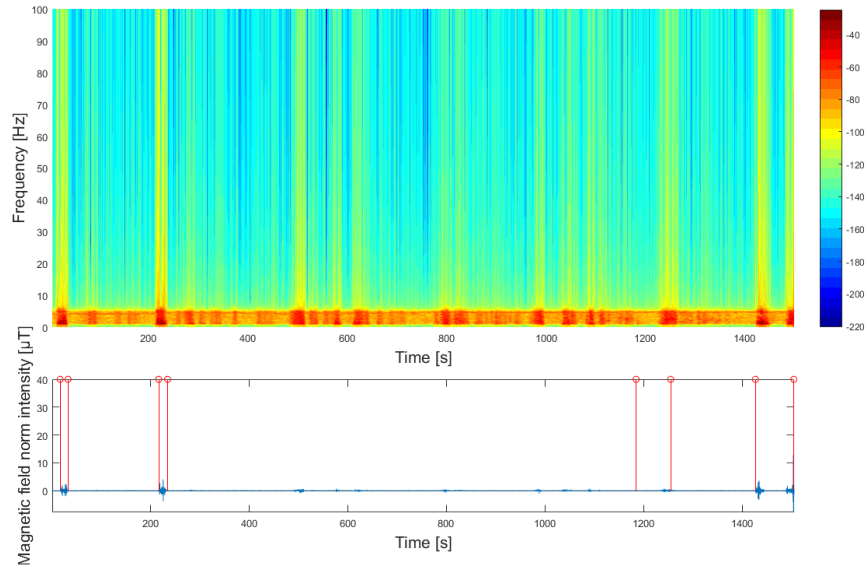


Figure 5.4: Spectral analysis of the PNI sensor in sensor element 11, after the filtering phase. The train disturbances are now the most powerful signals over the complete recording.

$G_n(\omega)$ of the n^{th} order Chebyshev filter, function of the angular velocity, is

equal to

$$G_n(\omega) = \frac{1}{\sqrt{1 + \epsilon^2 T_n^2\left(\frac{\omega}{\omega_0}\right)}}, \quad (5.1)$$

where ϵ, ω_0 and T_n are respectively the ripple factor, the cutoff frequency and the Chebyshev considered polynomial of the n^{th} order. Similarly, the type II Chebyshev filters are defined as

$$G_n(\omega) = \frac{1}{\sqrt{1 + \frac{1}{\epsilon^2 T_n^2\left(\frac{\omega}{\omega_0}\right)}}} \quad (5.2)$$

The filtering phase has been implemented in software using MATLAB. The filter parameter have been chosen in order to minimize the disturbance frequency gain [18].

5.3 Results and Discussion

The results from the PNI and the KMX sensor are extremely similar. The only real difference is the noise floor outside the train passage time-window, which is approximately $0.2 \mu\text{T}$ for the KMX sensor and $0.05 \mu\text{T}$ for the PNI sensor. As all other properties are almost equal, the result discussion is performed for the PNI sensors only, to avoid repetitions. All conclusions drawn for the PNI sensors hold for the KMX sensors too.

The first train transit is shown in Figure 5.5. The first transit is here taken as example to discuss the general disturbance behavior: a few considerations are made over the magnetic field variance pattern. All the eleven sensor elements record the same magnetic disturbance pattern in a synchronized way. The signal amplitude is scaled according to the sensor distance from the passing train. This pattern is very different from the one generated by the electric current, which is shown in Figure 5.6. The current pattern has no regular periodic behavior across the sensors, and also the amplitude varies in a chaotic and unpredictable way. In some way this behaviour helps in identifying the train transit, as the pattern is extremely similar across the array. It is worth noticing that all the four recorded train passages had different magnetic patterns, both in amplitude and for the general trend. Further data recording and analysis is needed to determine if the differences are due to the train speed, shape, a combination of the two or some other factor. What is possible to conclude from this experiment is that a neighboring train has a specific general pattern which is very different from the magnetic disturbances generated by the electric currents. Further on, it is likely that this pattern can be exploited in a detector, after appropriate signal filtering.

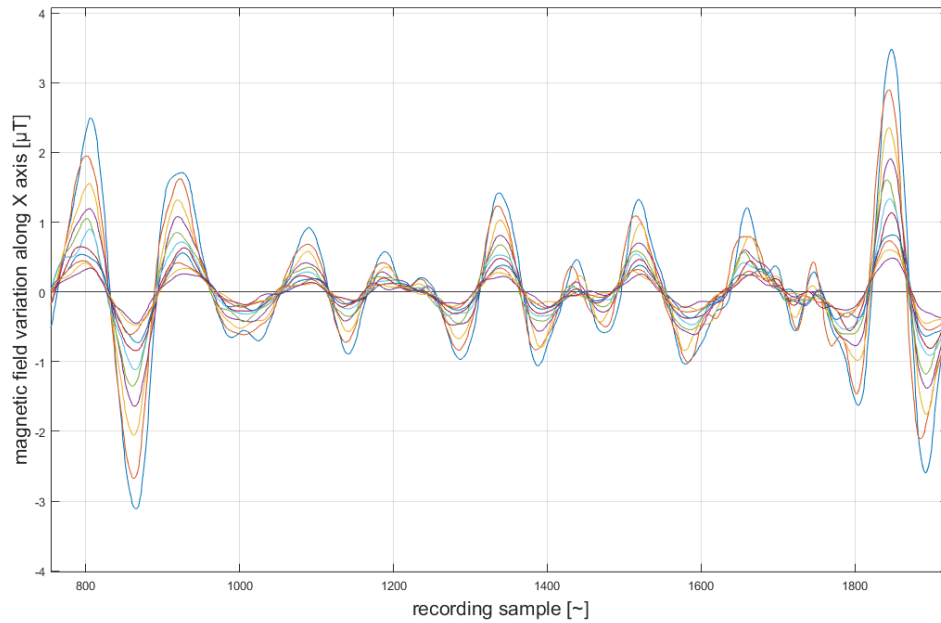


Figure 5.5: Filtered magnetic disturbances caused by the train 1 transit, for all PNI sensors.

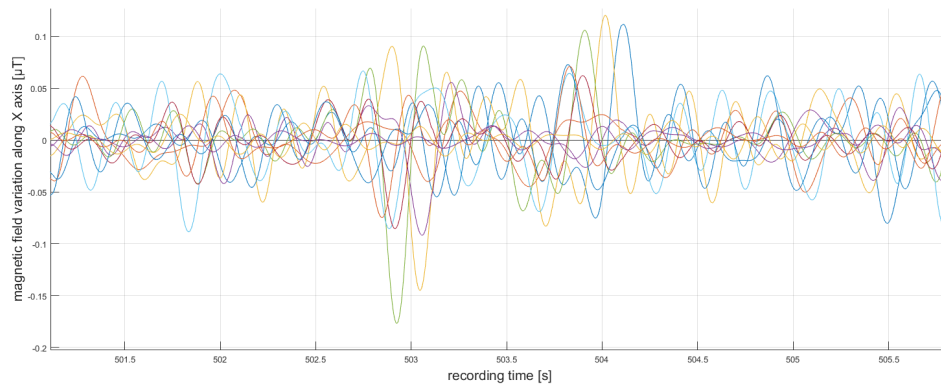


Figure 5.6: Filtered magnetic disturbances caused by residual current influence, for all PNI sensors.

The magnetic disturbance of a neighboring train fades along the cross-track direction. On the sensor element closest to the neighboring train, the magnetic disturbance has an amplitude comparable to the maximum variations recorded for a standard magnetic signature in railway environment [2]. The sensor that is the closest to the neighboring train is overwhelmed by the magnetic interference. Figure 5.7 shows how the magnetic influence of the recorded train passages decreases as the distance from the train increases. For all recorded passages, the residual magnetic influence at the opposite

end of the MSAS is equal to or smaller than $1 \mu\text{T}$.

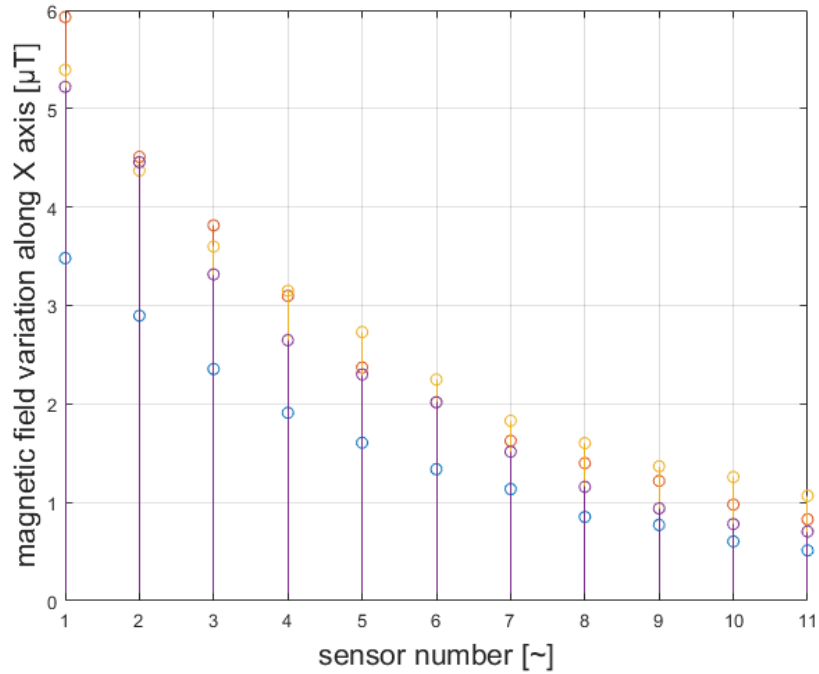


Figure 5.7: Maximum magnetic field disturbance recorded during each of the four train transits, for all PNI sensors.

Figure 5.8 shows the magnetic influence decay normalized to the value recorded by the closest sensor element, for each train passage. On the opposite side of the MSAS the residual magnetic influence of the neighboring train is decreased from 75% to 85%. It is worth noticing that this reduction is referred to the peak value, while the mean residual magnetic influence is indeed smaller.

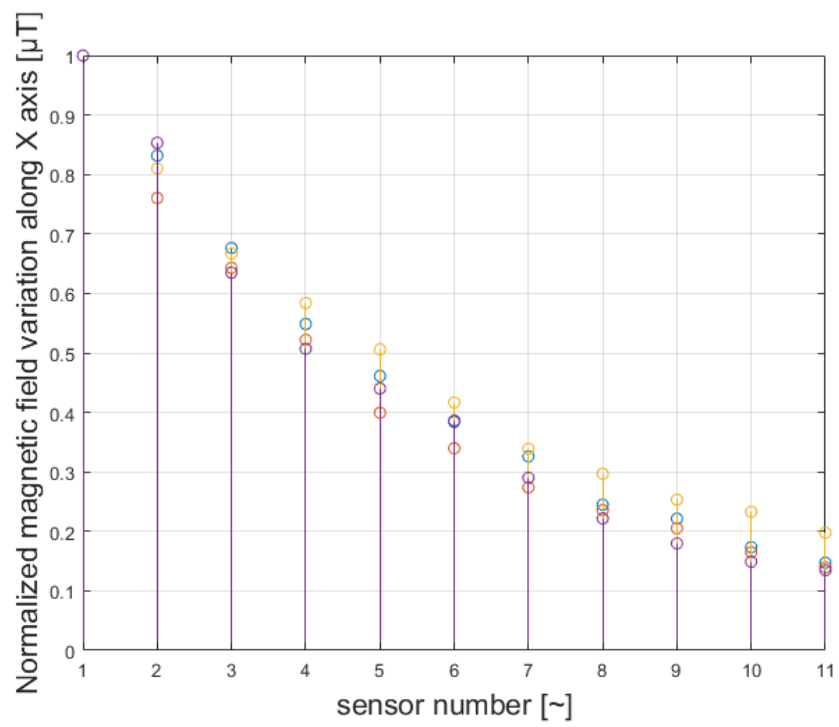


Figure 5.8: Normalized maximum magnetic field disturbance recorded during each of the four train transits, for all PNI sensors.

Chapter 6

Conclusions

The MSAS has been designed, built and tested during this work of thesis. This system is a train localization system, based on magnetic sensors, and it requires no additional infrastructure component on the track-side. The system contains eleven sensor element units, all equipped with two different low-cost magnetic sensors. Two experiments have been conducted and evaluated: the first is about magnetic localization with multiple sensors, and the second analyzes the magnetic disturbance caused by a neighboring train.

The first experiment pointed out that low-cost magnetic sensors are feasible for localization, especially when a multiple sensor system is used: the MSAS achieved accurate localization for more than 99% of the estimated positions. In the same experiment, the combined use of multiple sensors increased remarkably the overall correct localization probability: for the most relevant scenario, the accuracy gain is between 15% and 20% with respect to the single sensor system. Important considerations were also made about the localization methods: the $L1$ signal difference method (Manhattan difference) outperforms the cross-correlation methods, for both single sensor and multiple sensor systems. This result suggest that cross-correlation method is not suited for magnetic localization as should not be used in future related works.

The first experiment was performed in an automotive environment, with the MSAS mounted on a car. The magnetic signature was measured over a two-lane road about 360 m long. In this context, The MSAS could provide accurate localization exploiting the magnetic sensors, reaching performances comparable to a GNSS based localization system. The car test showed that magnetic localization should be followed up in automotive research context.

The second experiment showed a decay of the magnetic disturbance caused by a neighboring train along the cross-track direction. The experiment results showed that a neighboring train produces a specific pattern, which is measurable by a multiple magnetic sensor system such as the MSAS. The disturbance decay and pattern can be exploited for the disturbances de-

tection and exclusion in a magnetic localization system based on magnetic signature method.

Future works might profit from experimental data obtained from real-case scenarios. The evaluated experiments have shown that the MSAS is a localization system with excellent accuracy. The next research steps are the application to the MSAS to both railway and automotive environment for localization purposes, especially in contexts where GNSS based systems might not be available, such as tunnels or urban canyons.

Bibliography

- [1] C.J. Riley. *Encyclopedia of Trains and Locomotives*. MetroBooks, 2002.
- [2] O. Heirich and B. Siebler. Train-side passive magnetic measurements. In *IEEE International Instrumentation and Measurement Technology Conference*, pages 687–692, Pisa, Italy, May 2015. IEEE.
- [3] O. Heirich, B. Siebler, and H. Hedberg. Study of train-side passive magnetic measurements with applications to train localization. *Hindawi Journal of Sensors*, 2017.
- [4] O. Heirich and B. Siebler. Onboard train localization with track signatures: towards GNSS redundancy. In *ION GNSS+ 2017*, pages 687–692, Portland OR, USA, September 2017. The Institute of Navigation, Satellite Division.
- [5] D. Lu and E. Schnieder. Performance evaluation of GNSS for train localization. *IEEE Transactions of intelligent transport systems*, 16, 2015.
- [6] G. Barbu. GNSS/GALILEO certification for railway safety applications railway requirements and the strategic position of uic. In *World Congress of Rail Research*, Paris, France, 2008. UIC - International Union of Railways.
- [7] S. Hensel, C. Hasberg, and C. Stiller. Probabilistic rail vehicle localization with eddy current sensors in topological maps. *IEEE Transactions of intelligent transport systems*, 12(4):1525–1536, 2011.
- [8] A. Geistler. Train location with eddy current sensors. *CompRail, WIT Press*, May 2002.
- [9] Wikipedia contributors. CAN bus — Wikipedia, the free encyclopedia. https://en.wikipedia.org/w/index.php?title=CAN_bus&oldid=889563751. [Online; accessed 20-March-2019].
- [10] Wuntronic GmbH. Miniatur fluxgate magnetometer WFG-130. <https://www.wuntronic.de/en/miniatur-fluxgate-magnetometer-wfg-130.html>. [Online; accessed 20-March-2019].

- [11] PNI. PNI RM3100.
<https://www.pnicorp.com/rm3100/>. [Online; accessed 20-March-2019].
- [12] Kionix Inc. KMX62 - 1031.
<https://www.kionix.com/product/KMX62-1031>. [Online; accessed 20-March-2019].
- [13] ATMEL. AT90CAN128 datasheet.
<https://www.microchip.com/wwwproducts/en/AT90CAN128>. [Online; accessed 20-March-2019].
- [14] XSENS. XSens MTi-1.
<https://www.xsens.com/products/mti-1-series/>. [Online; accessed 20-March-2019].
- [15] MikroElektronika. Click board.
<https://www.mouser.it/new/mikroe/mikroelektronikaClick/>. [Online; accessed 20-March-2019].
- [16] ublox. ublox EVK-M8.
<https://www.u-blox.com/en/product/evk-8evk-m8>. [Online; accessed 20-March-2019].
- [17] National Marine Electronics Association. NMEA standards.
https://www.nmea.org/content/nmea_standards/v411.asp. [Online; accessed 20-March-2019].
- [18] A. Oppenheim, R. Schafer, and J. Buck. *Discrete-time signal processing*. Prentic Hall, 1999.
- [19] T.K. Moon and W.C.Stirling. *Mathematical Methods and Algorithms for Signal Processing*. Prentic Hall, 2000.
- [20] V. Moghtadaiee and A. Dempster. Vector distance measure comparison in indoor location fingerprinting. In *International Global Navigation Satellite Systems Society IGNSS Symposium*, Outrigger Gold Coast, Qld, Australia, July 2015.
- [21] X.R. Li, Y. Zhu, J. Wang, and C. Han. Optimal linear estimation fusion .i. unified fusion rules. *IEEE Transactions on Information Theory*, 49, 2003.
- [22] B. W. Parkinson and J. J. Spilker Jr. *Global Positioning System: Theory and Applications*, volume 1. American institutes of Aeronautics and Astronautics, Inc., 2 edition, 1994.
- [23] P. Misra and P. Enge. *Global Positioning System*. Ganga-Jamuna Press, 2 edition, 2006.

- [24] R. W. Daniels. *Approximation methods for electronic filter design: with applications to passive, active, and digital networks*. McGraw-Hill, 1974.